APPLICATION OF JPSS IMAGERS AND SOUNDERS TO TROPICAL CYCLONE TRACK AND INTENSITY FORECASTING

Galina Chirokova[1], Mark DeMaria[2], Robert DeMaria[1], and Jack Dostalek[1]

[1] CIRA/CSU, Fort Collins, CO, USA [2] NOAA/NESDIS/STAR, Fort Collins, CO, USA

Abstract

The time scale of tropical cyclone (TC) track and intensity changes is on the order of 6-12 hours, which makes Joint Polar Satellite System (JPSS) instruments well suited for the analysis and forecasting of these parameters. We are developing two TC applications of JPSS data. The first is using temperature and moisture retrievals from Advanced Technology Microwave Sounder (ATMS) in the near storm environment to improve intensity analysis and forecasting. The Maximum Potential Intensity (MPI) estimate, which is one of the key parameters in the operational Logistic Growth Equation Model (LGEM) and the related Rapid Intensification Index (RII), is calculated using ATMS data. Testing with a preliminary dataset shows up to 3.1% Brier Skill Score (BSS) improvement in the RII forecast relative to using model data to estimate the MPI. Possible improvements to LGEM are also discussed. The second application is using ATMS data for improving the center location estimate, which is the starting point for TC forecasts. Preliminary results for the years 2006-2011 (total of 2012 cases) (using AMSU as a proxy for the ATMS) showed 10% improvement in accuracy in comparison to the best storm center estimates available in real time. Methods are being developed to use multi-spectral imagery from Visible Infrared Imaging Radiometer Suite (VIIRS), including the low-light imager, in combination with ATMS sounder data to further refine accuracy of center-fix.

INTRODUCTION

Improving tropical cyclone (TC) track and intensity forecasts will lead to improved warnings and longer lead times for mitigation activities from TCs. The Suomi National Polar-Orbiting Partnership satellite (SNPP) launched in October, 2011, is part of the Joint Polar Satellite System (JPSS), the next generation polar-orbiting operational environmental satellite system. SNPP carries five instruments, including Visible Infrared Imaging Radiometer Suite (VIIRS) and Advanced Technology Microwave Sounder (ATMS). The time scale of TC track and intensity changes is on the order of 12 hours, which makes JPSS instruments well suited for the forecasting of these parameters.

Two basic methods exist for improving TC forecasts with SNPP. The first is to assimilate data in numerical forecast models, and the second is to improve analysis and statistical post-processing forecast products. Our group is developing two applications, focusing on the later approach. The first approach uses temperature and moisture retrievals from ATMS in the near storm environment to improve intensity analysis and forecasting. This new information is being incorporated into existing intensity estimation techniques and to operational statistical-dynamical intensity forecast models, including the Logistic Growth Equation Model (LGEM), to improve their performance. The second uses VIIRS and ATMS data for improving center location estimates of TCs, which is the starting point for TC forecasts. Methods are being developed to use multi-spectral imagery from VIIRS, including the low-light imager, in combination with sounder data for this purpose. These new products will be made available in the satellite Proving Ground to operational forecasters at the National Hurricane Center (NHC) and Joint Typhoon Warning Center (JTWC) for evaluation and feedback. If the evaluation is positive, the products can be transitioned to NHC and JTWC operations.

The paper is organized in the following way: 1) in the “data and methods” section we describe ATMS retrievals used for this study, and in the sections 2) and 3) we discuss the results obtained for each of the two applications.

DATA AND METHODS

ATMS represents a significant improvement in temperature and moisture retrievals over the current Advanced Microwave Sounding Unit (AMSU) instrument. Finer resolution and wider scan swath width result in better and more frequent TCs observations, along with a larger number of usable soundings. Compared to AMSU, ATMS has almost twice the resolution at nadir (26 km ATMS vs. 52 km AMSU) in some channels, and the ATMS swath width is 2503 km compared to the 2200 km AMSU swath width. The most important improvement for TC applications is that ATMS has temperature and moisture sounding channels combined on the same instrument, including one new temperature channel (51.7 GHz) for sounding the lower troposphere, and two new moisture channels (183 +- 1.8 GHz and 183 +- 4.5 GHz), which were not previously available on AMSU. Further details of ATMS instrument could be found in Weng et al. (2012). In addition to the new instrument, ATMS data are processed with the new MIRS retrieval scheme (Boukabara et al., 2011), which offers several advantages over the current operational statistical retrievals. Thus, ATMS-MIRS is better resolving the TC warm core, and the simultaneous retrieval of temperature and moisture profiles allows significant reductions in the artificial cooling in the areas of high cloud liquid water and ice scattering, which are strongly affecting statistical AMSU retrievals (Bessho et al., 2006; Demuth et al., 2004).

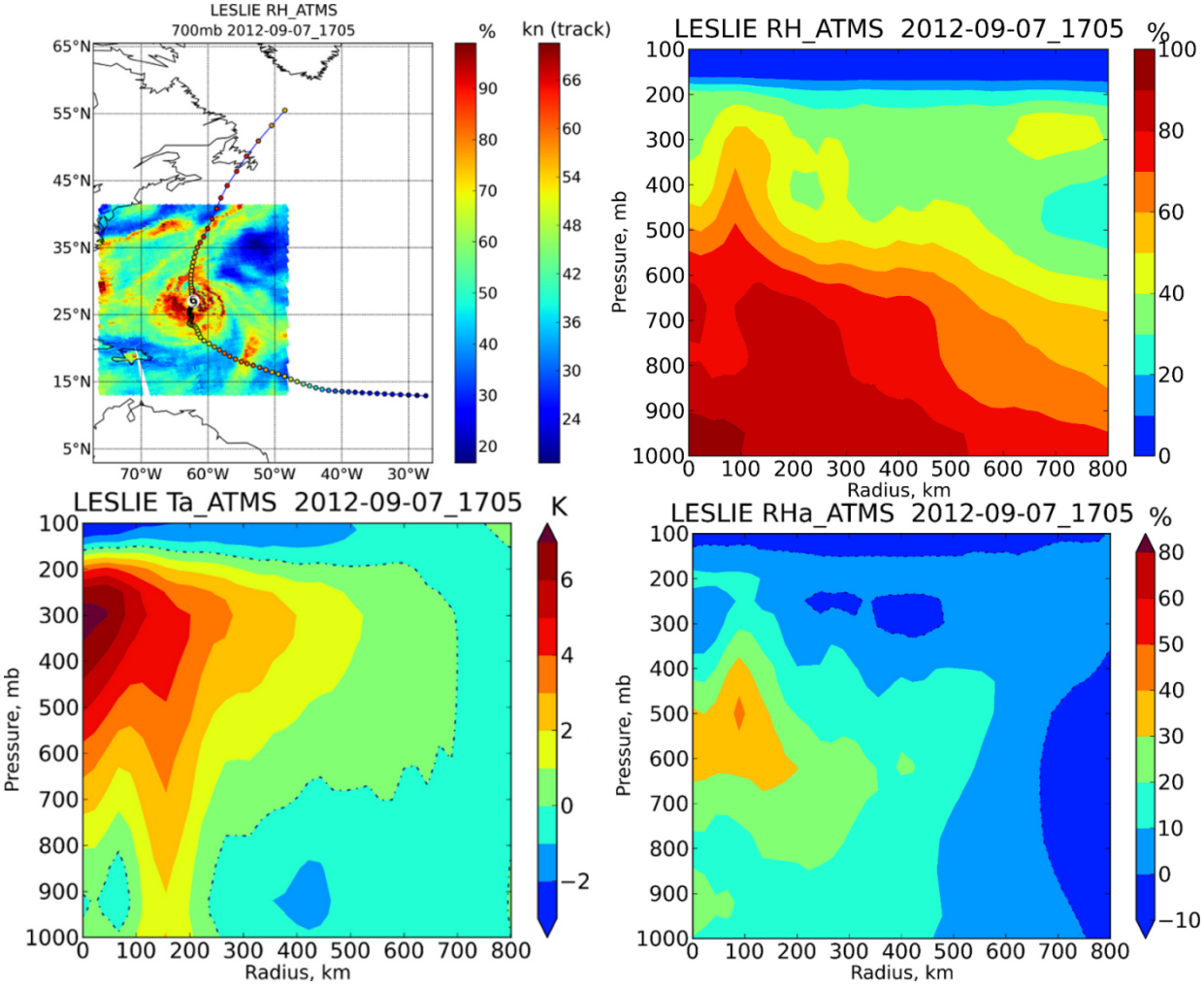

Figure 1. **ATMS MIRS temperature and moisture retrievals for a case from Hurricane Leslie, including the 700 hPa relative humidity field (RH) (upper left), and radial-height cross sections of RH (upper right), temperature anomaly (lower left) and RH anomaly (lower right).**

The MIRS temperature and moisture retrievals are not yet operational, however, a large sample of cases produced using the same algorithm and in the same format as will be available operationally were obtained from K. Garrett from NESDIS/STAR. This sample includes 43 days for 23 TCs from

2012, providing over 200 cases from global TCs. This dataset is being used for the majority of the algorithm testing described below.

In the MIRS retrievals the water vapor is retrieved in terms of mixing ratio. We developed methods to convert it to relative humidity (RH), analyze the data in storm-centered coordinates, perform azimuthal averages, and generate perturbation fields. Figure 1 shows an example of a 700 hPa RH field for Hurricane Leslie from the 2012 Atlantic season (upper left). The temperature anomaly plot (lower left) shows a very realistic warm core structure, which does not require low-level correction for high cloud liquid water (CLW) and ice scattering (Demuth et al., 2004). The structure of the moisture fields, the radial-height cross sections of the azimuthally averaged RH (upper right), and RH anomaly (lower right) look very reasonable, with RH increasing near the storm center. Preliminary comparison shows that RH values at 600km from the storm center are similar to Jordan mean tropical sounding (Dunion et. al, 2008), and RH values near the center of the storm are similar to dropsondes data (not shown).

MAXIMUM POTENTIAL INTENSITY ESTIMATE

TC track errors have improved dramatically over the past few decades, primarily due to improvements in data assimilation and forecast models. However, the ability to forecast intensity changes has improved much more slowly (DeMaria, 2007). An especially difficult but very important forecast problem, in particular for storms close to land, is predicting rapid changes in TC intensity. Improving these forecasts is one of the highest priorities within NOAA. Because of the importance of this problem, an operational tool called the Rapid Intensification Index (RII) has been developed (Kaplan et al, 2010). The RII uses a subset of the input to LGEM forecast in a discriminate analysis algorithm to estimate the probability of rapid intensity changes.

.

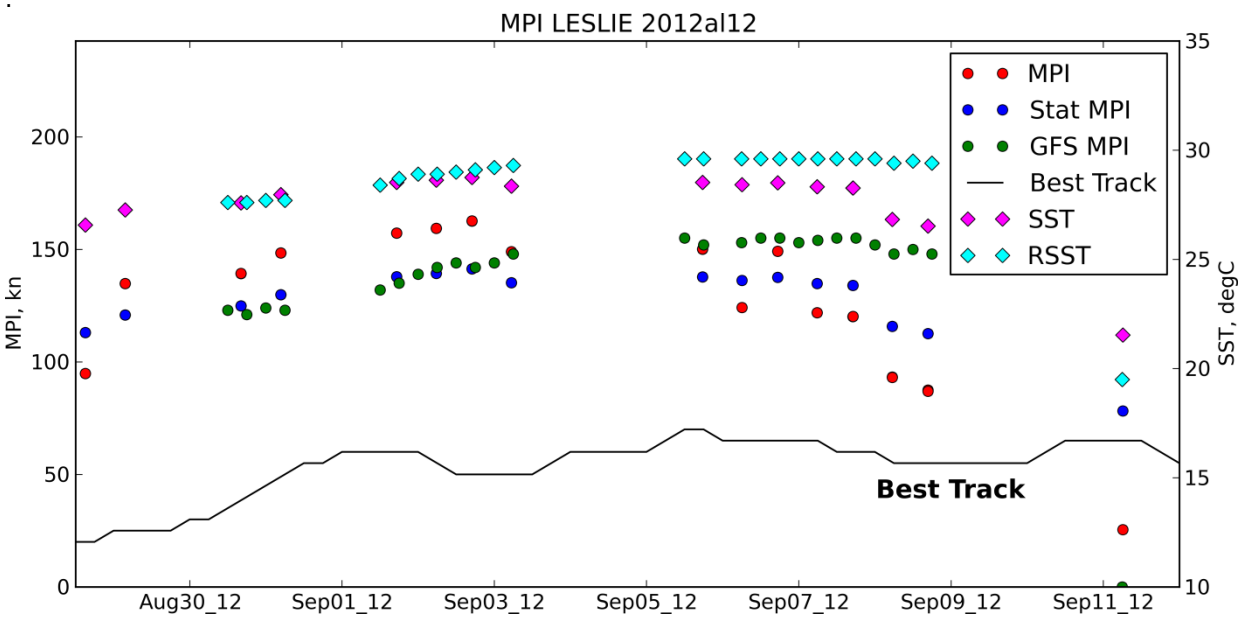

***Figure 2*: MPI estimate for hurricane Leslie (AL12). Upper panel: Best Track intensity (black line), ATMS MPI at swath times (red dots) and GFS MPI at synoptic times (green dots). Also statistical MPI (blue dots) NCODA SST (magenta diamonds) and Reynolds SST used by operational LGEM (cyan diamonds) are shown.**

The accuracy of the LGEM forecast, the most accurate of the statistical models over the past few years, critically depends on the accuracy of the Maximum Potential Intensity (MPI) estimate. Currently, the operational LGEM and RII at National Hurricane Center (NHC) use the MPI calculated from a simple statistical algorithm (DeMaria and Kaplan, 1994), which only uses SST data and does not take into account temperature and moisture soundings. We investigate the use of ATMS-MIRS retrievals as input into the more general Bister and Emanuel (1998) MPI algorithm to improve RII forecast. Following Emanuel (1988) and Bister and Emanuel (1998), MPI can be calculated from ATMS-MIRS T,Q, and SLP together with SST data as

$$(MPI) = \frac{T_s - T_o}{T_o} \frac{C_k}{C_D} (k^* - k),$$

where T_s and T_o are the surface temperature and the temperature at the outflow level; k* and k are the saturation enthalpy of the sea surface and the actual enthalpy of the boundary layer air, respectively; and C_k/C_D is the specified ratio of surface exchange coefficients for momentum and enthalpy. T_s,T_o, k*, and k are estimated from soundings and SST.

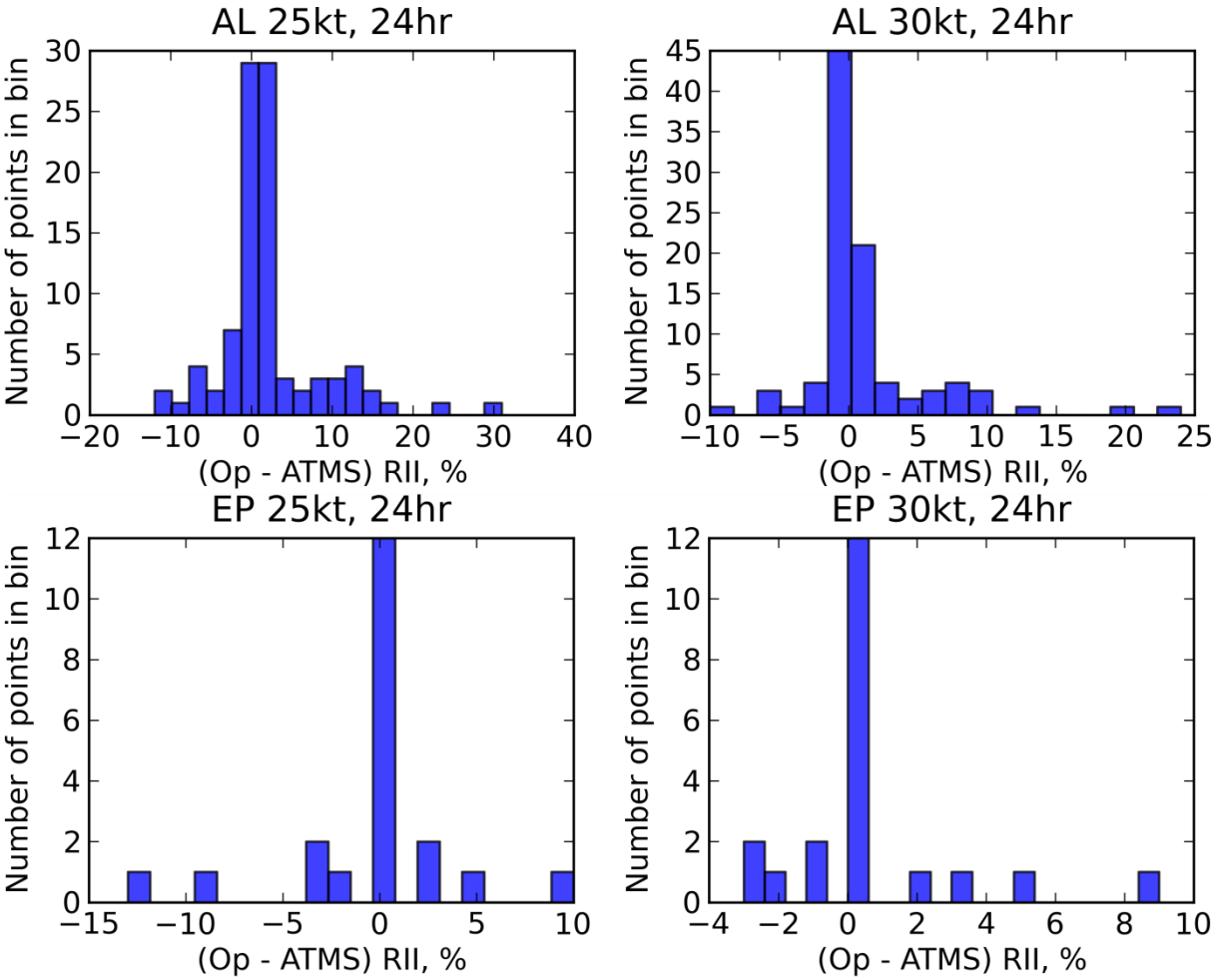

Figure 3: Histogram of the differences between operational RI probabilities and RII calculated with ATMS MPI. Two upper panels show probabilities for the Atlantic Basin for 25kt (left) and 30kt (right), and two lower panels show corresponding probabilities for East Pacific Basin.

Algorithms were developed to calculate ATMS temperature and RH soundings, and the MPI algorithm was successfully adapted to use as input the ATMS retrievals together with the U.S. Navy Coupled Ocean Data Assimilation (NCODA) SST analysis (Cummings, 2005). Values were calculated for all cases in the preliminary MIRS dataset. Figure 2 shows a comparison of the MPI estimates from three methods for Hurricane Leslie from 2012 Atlantic season, including the empirical MPI currently used by NHC's statistical intensity models (dark blue circles), the MPI calculated from Bister and Emanuel (1998) theoretical formula with storm environmental soundings from the Global Forecast System (GFS) analysis (green circles), and the MPI calculated from the same formula with environmental soundings from ATMS (red circles). Also shown in this figure are two SST values, the weekly Reynolds SST (Reynolds et al., 2007) and that from the daily NCODA analyses. The Reynolds SSTs were used to calculate the model MPI, and NCODA SSTs were used to calculate statistical MPI and MPI from MIRS retrievals. There are significant differences between the MPI results, with the MIRS input resulting in higher values for warmer SSTs and lower values for colder SSTs, as compared to both the statistical and GFS MPI estimates.

The Rapid Intensification Index (RII, Kaplan et al., 2010) has also been adapted to run with the new MPI estimates with ATMS. RII is calculated based on current MPI and four predicted MPI values at 6 h intervals along the forecasted storm track. As the initial value we used the calculated ATMS MPI, and as predicted values we used GFS MPI corrected by the initial difference between the ATMS and GFS MPI values. In order to evaluate RII forecast, we need to exclude all extratropical cases, as well as cases that are too close to the land. As result, we have a very small number of cases to work with: 100 cases for the Atlantic Basin and only 22 cases for the East Pacific Basin. That number of cases is not sufficient to calculate reliable forecast statistics, so the results presented below are preliminary.

Before comparing the RII forecasts to ground truth, we first tested the sensitivity of the probabilities to the differing methods for calculating the MPI. Figure 3 shows histograms of the changes in the probability of rapid intensification that results from replacing the GFS MPI with the ATMS MPI, for two different RI thresholds (25 and 30 kt increases in 24 hr) for the Atlantic and East Pacific. This figure shows that there is considerable forecast sensitivity to the MPI calculation, where the RII probability changed by up to 30%. A larger data set with the addition of the western North Pacific Basin is being tested to provide a larger statistical sample for evaluation.

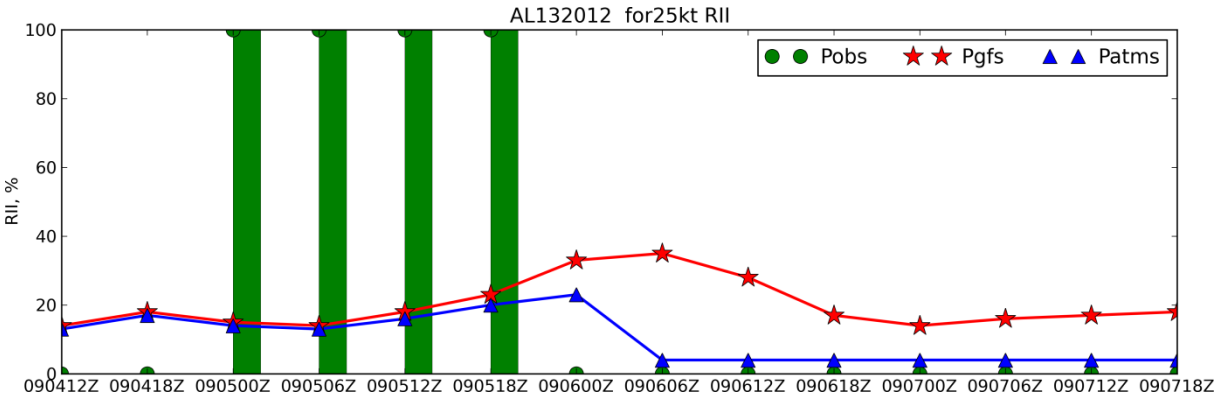

Figure 4: RII for 25 knots for Hurricane Michael, AL13 2013. Green dots show observed RII index, which is 0 if no RI occurred, and 100% if RI occurred. Blue line with triangles shows RI forecast based on operational GFS model fields, and red line with stars shows RI forecast with MPI calculated from ATMS data. The bias of ATMS data is 1.67 compared to 1.87 bias from GFS.

Figure 4 shows observed and predicted 25 Kt RII for major hurricane Michael, AL13, 2012. The green bars indicate times for which RI occurred in next 24 hours. Red and blue stars/triangles show RII predicted based on MPI calculated from GFS fields (red) and from ATMS retrievals (blue). Although both RI estimates are somewhat late, the ATMS-based RII goes down much quicker after hurricane intensification ended, thus contributing to lower bias and higher Brier Skill Score (BSS). A similar relationship is observed for other RII cases in Atlantic (not shown).

	Atlantic		
	Bias		BSS(ATMS/GFS)
RI	GFS	ATMS	
25 kt	1.87	1.67	1.27%
30 kt	1.43	1.26	1.55%
35 kt	1.45	1.25	3.00%
40 kt	1.93	1.60	3.14%

Table 1: Bias for Atlantic and Brier Skill Score for Atlantic and East Pacific basins. Bias is always smaller for RII estimate from ATMS data as compared to GFS. Brier Skill Score increases by 1 – 3 % by using ATMS data for Atlantic Basin, and show increase for all RI except 25kt for EP. All numbers for the Atlantic basin are based on very small sample size (100 cases) and could possibly change as more data become available.

As can be seen from Table 1, the bias is always smaller for RII estimate from ATMS data as compared to GFS. Brier Skill Score (BSS) increases by 1 – 3 % by using ATMS data for the Atlantic Basin. Preliminary results for East Pacific basin also show BSS increase for all RI thresholds except

for 25kt (not shown). Estimates for the Atlantic are based on very small sample size (100 cases) and could possibly change as more data become available.

CENTER-FIX ALGORITHM

When a TC has formed, typically the first step in producing a forecast is to perform a center-fix to estimate the location of the center of the storm. An accurate center estimate is necessary to prevent initial errors from impacting later steps in forecast production. While aircraft reconnaissance can be used to produce highly accurate center estimates, only about 30% of all TC forecasts have aircraft data available for their production in the Atlantic, and most other TC basins have no aircraft data. Satellite data is available at a much higher rate; however, most of the existing center-fix algorithms are subjective, and due to the limited amount of time that forecasters have to perform prediction for TCs, satellite imagery is an underutilized resource for performing center-fixing. The only existing objective center-fix algorithm developed by Wimmers and Velden (2010) is primarily using spiral patterns in microwave imager data, but does not use microwave sounder data. Our technique uses microwave sounder data, which provides a more physical representation of a cyclone, to estimate pressure, and is novel in its use of techniques from the field of machine learning. Additionally, one of the aims of the proposed method is to improve performance for weak storms.

Using the hydrostatic integration of AMSU MIRS temperature retrievals, the proposed algorithm poses the center-fixing problem as a variation of a classification problem. That is, using a grid-cell in an AMSU retrieval as input, the output of the algorithm should be a value indicating the probability that the grid-cell contains a storm center (class A) and a value indicating the probability that the grid-cell does not contain a storm center (class B). Due to its relative ease to implement, Quadratic Discriminant Analysis (QDA) was selected as the algorithm to perform the classification (Bishop, 2006). In order to perform the classification, QDA must be trained. A large dataset of statistical AMSU retrievals, from 2006-2011, was used to train the algorithm. The dataset was assembled by randomly selecting 70% of the available retrievals from 2006-2011 and further selecting only cases that had times that fit between the beginning and end of the appropriate NHC best-track file. Additionally, only retrievals where the storm under examination had maximum winds over 35 kt were included. The retrievals within the remaining 30% of available data that met the same criteria were selected to be the test data set. The training set consisted of 1605 AMSU retrievals and the testing set consisted of 416 AMSU retrievals.

A small dataset of ATMS-MIRS retrievals from 2012 was also made available for use with this algorithm. Using the same method as described above, a training set of 146 ATMS retrievals and a testing set of 90 ATMS retrievals were assembled. Additionally, a testing set using all 236 ATMS retrievals was assembled for use with the AMSU training set.

For each retrieval, a 5x5 grid-cell area around the real-time center fix provided by the NHC forecast from the first synoptic time before the time of the AMSU data (referred to as the extrapolated point) was selected. The grid contains the 700 hPa geopotential height fields determined from the hydrostatic integration of the AMSU or ATMS retrievals. The grid spacing is 0.2 latitude/longitude. The center-location reported by the NHC best-track was then calculated by generating a spline path through the locations in the appropriate best-track file and finding the interpolated position corresponding to the retrieval time. Further, each grid-cell was examined to determine if the best-track center position was located within the grid-cell and marked as the appropriate class. Using this training dataset, QDA was used to generate a function for each of the two classes relating the input values to the probability that they belong to that class. These functions are referred to as discriminant functions. The inputs to the discriminant functions are the geopotential height field and several parameters derived from it, such as the distance from the height minimum and the magnitude of the horizontal height gradient. Once these two functions have been generated, center-fixes can then be performed using retrieval data. To perform a center-fix, a 5x5 grid-cell area around the extrapolated point is selected. The geopotential height field from these grid-cells are then used as input to both classifier (discriminant) functions. The value for the class B discriminant function is then subtracted from the value returned from the class A discriminant function for each grid-cell. The grid cell with the

maximum difference value is selected as the grid-cell that is most likely to contain the storm center for that retrieval.

To evaluate the performance of the center-fix algorithm we compare the distances from the storm center reported by NHC best-track to 1) the storm center estimated by our algorithm and 2) to the extrapolated position (baseline distance). Figure 5 shows the results of three tests which were performed to measure the performance of the center-fix algorithm: the AMSU trained algorithm run against the AMSU test set (AMSU-AMSU, blue bars), the 146 ATMS retrieval trained algorithm run against the 90 ATMS retrieval test set (ATMS-ATMS, red bars), and the AMSU trained algorithm run against the 236 ATMS retrieval test set (AMSU-ATMS, green bars). The real-time center fixes for the AMSU-AMSU test had a mean error of 0.451 degrees, while the output of the center-fix algorithm produced a mean error of 0.400 degrees. The real-time center fixes for the ATMS-ATMS had a mean error of 0.604 degrees compared to the center-fix algorithm mean error of 0.520 degrees. The real-time center fixes for the AMSU-ATMS test had a mean error of 0.587 degrees and the center-fix algorithm had a mean error of 0.477 degrees. So for the AMSU-AMSU, ATMS-ATMS, and AMSU-ATMS tests the center-fix algorithm saw an improvement over the real-time extrapolated center fixes of 11%, 14% and 19% respectively. It should be noted that the ATMS training and testing sets are very small and represent preliminary results. The ATMS training and testing sets will be expanded in the future as more ATMS data becomes available.

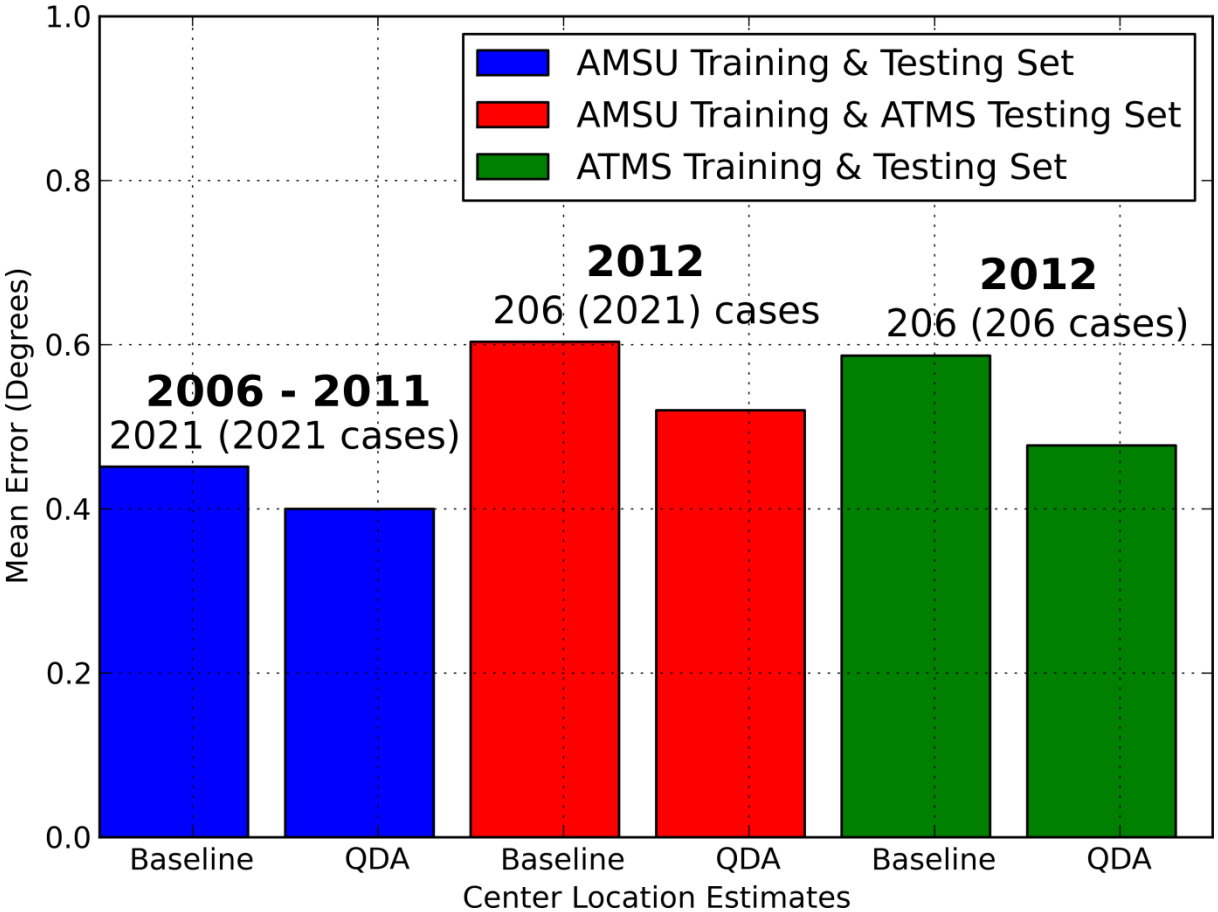

***Figure 5*: Errors in the center location estimate using the NHC best track positions interpolated to the time of the microwave pass. For each pair of bars (blue, red green), the left bar is the error of the first guess position and the second one is the error after the first guess has been updated using the quadratic discriminant analysis (QDA) technique. Results show that using the ATMS data provides a bigger improvement than the AMSU data, even for the case where the algorithm trained on AMSU data is used with ATMS input. The QDA will then be refined using the much higher resolution VIIRS data.**

CONCLUSIONS AND FUTURE PLANS

Preliminary results for the RII forecast show up to 3.1% increase in Brier Skill Score with the use of ATMS data, and for the center-fix algorithm up to 10% better center location as compared to the first guess position from the NHC real-time forecast positions. Both of these results are very encouraging, and will be further refined as more ATMS-MIRS data become available. LGEM and RII intensity forecasts are critically dependent on MPI estimate, and the impact of ATMS-calculated MPI on LGEM is being investigated. The next step in the center-fix algorithm is the addition of VIIRS data, especially the Day Night Band (DNB) data, to refine the estimates from the microwave sounder input. Finally, both the intensity and center-fix algorithms could be further improved by using Cross-Track Infrared Sounder (CrIS) data.

REFERENCES

Bessho, K., M. DeMaria, and J. Knaff, 2006: Tropical Cyclone Wind Retrievals from the Advanced Microwave Sounding Unit: Application to Surface Wind Analysis. J. Appl. Meteor. Climatol., **45**, 399–415. doi: 10.1175/JAM2352.1

Bishop C.M., 2006: Pattern Recognition and Machine Learning, New York, NY, Springer Science+Business Media, LLC, 749pp.

Bister, M., and K. A. Emanuel, 1998: Dissipative heating and hurricane intensity. Meteor. Atmos. Phys., **65**, 233–240. doi:10.1007/BF01030791

Boukabara, S.-A., K. Garrett, W. Chen, F. Iturbide-Sanchez, C. Grassotti, C. Kongoli, R. Chen, Q. Liu, B. Yan, F. Weng, R. Ferraro, T. Kleespies, and H. Meng, 2011: MiRS: An All-Weather 1DVAR Satellite Data Assimilation & Retrieval System. IEEE Trans. Geosci. Remote Sens., **49**, no. 9, pp. 3249-3272, Sep. 2011. doi: 10.1109/TGRS.2011.2158438

Cummings, J. A., 2005: Operational multivariate ocean data assimilation. Quart. J. Roy. Meteor. Soc., **131**, 3583–3604.

DeMaria, M., J. Kaplan, 1994: Sea Surface Temperature and the Maximum Intensity of Atlantic Tropical Cyclones. J. Climate, **7**, 1324–1334.doi: http://dx.doi.org/10.1175/1520-0442(1994)007<1324:SSTATM>2.0.CO;2

DeMaria, M., J.A. Knaff, and C.R. Sampson, 2007: Evaluation of Long-Term Trends in Operational Tropical Cyclone Intensity Forecasts. Meteor. and Atmos. Physics, **97**, 19-28.

Demuth, Julie L., Mark DeMaria, John A. Knaff, 2006: Improvement of Advanced Microwave Sounding Unit Tropical Cyclone Intensity and Size Estimation Algorithms. J. Appl. Meteor. Climatol., 45, 1573–1581. doi: http://dx.doi.org/10.1175/JAM2429.1

Demuth, J. L., DeMaria, M., Knaff, J. A., Vonder Haar, T. H., 2004: Evaluation of Advanced Microwave Sounding Unit Tropical-Cyclone Intensity and Size Estimation Algorithms. J. Appl. Meteor., **43**, 282–296.doi: http://dx.doi.org/10.1175/1520-0450(2004)043<0282:EOAMSU>2.0.CO;2

Dunion, J. P. and C. S. Marron, 2008: A Reexamination of the Jordan Mean Tropical Sounding Based on Awareness of the Saharan Air Layer: Results from 2002. J. Climate, **21**, 5242–5253.doi: http://dx.doi.org/10.1175/2008JCLI1868.1

Emanuel, K. A., 1988: The Maximum Intensity of Hurricanes. J. Atmos. Sci., **45**, 1143–1155.doi: http://dx.doi.org/10.1175/1520-0469(1988)045<1143:TMIOH>2.0.CO;2

Kaplan, J., M. DeMaria, and J.A. Knaff, 2010: A revised tropical cyclone rapid intensification index for the Atlantic and east Pacific basins. Wea. Forecasting, **25**, 220-241.

Reynolds, R. W., T. M. Smith, C. Liu, D. B. Chelton, K. S. Casey, and M. G. Schlax, 2007: Daily high-resolution blended analyses for sea surface temperature. J. Climate, **20**, 5473-5496.

Weng, F., Zou, X., Wang, X., Yang, S., & Goldberg, M. D. 2012: Introduction to Suomi NPP ATMS for NWP and tropical cyclone applications. J. Geophys. Res, **117**, D19112,14PP. doi:1029/2012JD018144

Wimmers, A. J., C. S. Velden, 2010: Objectively Determining the Rotational Center of Tropical Cyclones in Passive Microwave Satellite Imagery. J. Appl. Meteor. Climatol., **49**, 2013–2034.doi: http://dx.doi.org/10.1175/2010JAMC2490.1